Kristen L. Zakian, PhD
Steven Eberhardt, MD
Hedvig Hricak, MD, PhD
Amita Shukla-Dave, PhD
Shanon Kleinman, BS
Manickam Muruganandham, PhD
Kanishka Sircar, MD
Michael W. Kattan, PhD
Victor E. Reuter, MD
Peter T. Scardino, MD
Jason A. Koutcher, MD, PhD

Index terms:
Magnetic resonance (MR), spectroscopy, 844.12145
Magnetic resonance (MR), tissue characterization, 844.12145
Prostate, hyperplasia, 844.316
Prostate, MR, 844.12145
Prostate, neoplasms, 844.32

Published online before print
10.1148/radiol.2291021383
Radiology 2003; 229:241–247

Abbreviations:
BASING = band-selective inversion with gradient dephasing
BPH = benign prostatic hyperplasia
Cho = choline-containing compounds
Cit = citrate
Cr = creatine/phosphocreatine
PRESS = point-resolved spectroscopy
PSA = prostate-specific antigen
PZ = peripheral zone
TZ = transition zone

[1] From the Departments of Medical Physics (K.L.Z., A.S.D., S.K., M.M., J.A.K.), Radiology (K.L.Z., S.E., H.H., J.A.K.), Pathology (K.S., V.E.R.), Urology (M.W.K., P.T.S.), Epidemiology and Biostatistics (M.W.K.), and Medicine (J.A.K.), Memorial Sloan-Kettering Cancer Center, 1275 York Avenue, New York, NY 10021. Received October 28, 2002; revision requested December 12; revision received January 15, 2003; accepted February 28. Supported by National Institutes of Health grants R21 CA 84258-01 and 7-R01 CA76423. **Address correspondence to** K.L.Z. (e-mail: *zakiank@mskcc.org*).

Author contributions:
Guarantor of integrity of entire study, K.L.Z.; study concepts, K.L.Z., H.H., S.E., P.T.S., V.E.R., J.A.K.; study design, K.L.Z., H.H., P.T.S., J.A.K., V.E.R.; literature research, K.L.Z.; clinical studies, V.E.R., K.S., P.T.S., H.H., S.E., K.Z., A.S.D., M.M.; data acquisition, A.S.D., M.M.; data analysis/interpretation, K.L.Z., S.E., S.K., K.S., M.W.K.; statistical analysis, M.W.K.; manuscript preparation, S.K., A.S.D., M.M., K.L.Z., H.H., S.E.; manuscript definition of intellectual content, K.L.Z., H.H.; manuscript editing, H.H., S.E., J.A.K., V.E.R., P.T.S., M.W.K., S.K., A.S.D.; manuscript revision/review, all authors; manuscript final version approval, H.H., J.A.K., S.E., K.L.Z.

© RSNA, 2003

Transition Zone Prostate Cancer: Metabolic Characteristics at ^{1}H MR Spectroscopic Imaging—Initial Results[1]

PURPOSE: To determine whether cancers of the prostate transition zone (TZ) possess a unique metabolic pattern by which they may be identified at proton magnetic resonance (MR) spectroscopic imaging.

MATERIALS AND METHODS: Findings in 40 patients who underwent combined endorectal MR imaging and hydrogen 1 MR spectroscopic imaging before radical prostatectomy and who had TZ tumor identified subsequently at step-section pathologic analysis were retrospectively reviewed. Within this population, a subset of 16 patients whose TZ tumor had a largest diameter of 1 cm or greater and was included in the MR spectroscopic imaging excitation volume was identified. In these 16 patients, the ratios of choline-containing compounds (Cho) and creatine/phosphocreatine (Cr) to citrate (Cit) (ie, [Cho + Cr]/Cit), Cho/Cr, and Cho/Cit were compared in tumor and control tissues. The presence of only Cho and the absence of all metabolites were also assessed.

RESULTS: The mean values of (Cho + Cr)/Cit, Cho/Cr, and Cho/Cit were different between TZ cancer and control tissues (P = .001, P = .003, and P = .001, respectively; Wilcoxon signed rank test). Nine (56%) of 16 patients had at least one tumor voxel in which Cho comprised the only detectable peak, while no control voxels showed only Cho (P = .008, McNemar test). The percentage of voxels in which no metabolites were detected did not differ between tumor and control tissues (P = .134, McNemar test).

CONCLUSION: TZ cancer has a metabolic profile that is different from that of benign TZ tissue; however, the broad range of metabolite ratios observed in TZ cancer precludes the use of a single ratio to differentiate TZ cancer from benign TZ tissue.

© RSNA, 2003

Magnetic resonance (MR) imaging and MR spectroscopic imaging have been gaining acceptance as tools in the evaluation of prostate cancer (1–10). Thus far, MR imaging and MR spectroscopic imaging assessment of prostate cancer has focused on the peripheral zone (PZ) of the prostate gland. Although 65% of prostate cancers arise in the PZ, up to 30% arise in the transition zone (TZ) (11). Evaluation of the TZ with imaging, including both MR imaging and ultrasonography (US), is difficult because the TZ is the site of origin of benign prostatic hyperplasia (BPH), which can have a heterogeneous appearance (12,13).

Proton MR spectroscopic imaging has been successfully applied to the diagnosis of cancer in the PZ on the basis of the elevation of choline-containing compounds (Cho) and the reduction of citrate (Cit) in cancerous tissue compared with normal, healthy PZ tissue (10,14–17). The ratio (Cho + Cr)/Cit, where Cr is creatine/phosphocreatine, has been used to aid in the diagnosis of cancer, and the combination of endorectal MR imaging and MR spectroscopic imaging has shown high sensitivity and specificity for detecting tumors of

the PZ (10). The goal of the current study was to determine whether cancers in the TZ possess a unique metabolic pattern by which they may be identified at proton MR spectroscopic imaging.

MATERIALS AND METHODS

Initial Patients and MR Data Acquisition and Processing

From January 2000 to January 2002, a total of 130 previously untreated patients underwent combined endorectal MR imaging and hydrogen 1 (^{1}H) MR spectroscopic imaging (hereinafter referred to as MR imaging/MR spectroscopic imaging) followed by radical prostatectomy and whole-mount step-section pathologic examination. MR imaging/MR spectroscopic imaging studies were performed with a 1.5-T Signa Horizon MR imaging unit (GE Medical Systems, Milwaukee, Wis) by using MR spectroscopic imaging software developed at the University of California at San Francisco (15,18–21). Informed consent was obtained from all patients according to a protocol that was approved by the institutional review board of our institution.

In the imaging portion of our study, transverse T1-weighted MR images were obtained from the aortic bifurcation to below the prostatic apex by using a spin-echo pulse sequence with the following parameters: repetition time msec/echo time msec, 700/14; field of view, 24 cm; section thickness, 5 mm; gap, 1 mm; and number of signals acquired, two. T2-weighted MR images in the transverse and coronal planes were acquired by using a fast spin-echo sequence with the following parameters: 4,000/102; echo train length, 12; field of view, 14 cm; section thickness, 3 mm; gap, 0 mm; and number of signals acquired, four. MR spectroscopic imaging consisted of point-resolved spectroscopy (PRESS) voxel excitation (22) with band-selective inversion with gradient dephasing (BASING) water and lipid suppression (18) and spatial encoding by chemical shift imaging (23) at 6.25-mm resolution in all three dimensions. Timing parameters were 1,000/130 and imaging time, 17 minutes.

Data processing was performed at a Sun Ultra 10 workstation (Sun Microsystems, Mountain View, Calif) and included 2-Hz Lorentzian spectral apodization, four-dimensional Fourier transform, and automated frequency, phase, and baseline correction (21). Spectral data were zero filled to 3.1-mm resolution in the superior-inferior dimension and overlaid on corresponding transverse T2-weighted MR images. Peak areas were calculated by using numeric integration. To provide a noise measurement, we calculated the SD of the MR signal intensity in a region of the spectrum containing only noise. Metabolite peak areas were then normalized with respect to the noise SD to yield an approximate signal-to-noise ratio.

Pathologic Examination and Final Patient Group

Prostatectomy was followed by specimen fixation in 10% formalin for 36 hours. The distal 5-mm portion of the apex was amputated and coned. The remainder of the gland was serially sectioned from the apex to the base at 3–4-mm intervals and entirely submitted for paraffin embedding as a "whole mount." The seminal vesicles were amputated and embedded separately. After paraffin embedding was performed, microsections were cut at 3-mm intervals, placed on glass slides, and stained with hematoxylin-eosin. Cancer foci were outlined in ink by a pathologist (K.S. or V.E.R.) on slides of the whole-mount, apical, and seminal vesicle slices so that the foci could be grossly seen and photographed. These photographs constituted the tumor maps. For the purposes of this study, tumors considered to arise in the TZ and tumors of PZ origin with a large component invading the TZ were included. For each patient, the Gleason scores for both the entire radical prostatectomy specimen and the TZ tumor, the pathologic stage, the zonal origin of the TZ tumor, and the presence or absence of synchronous PZ tumors were tabulated.

Forty patients with histopathologically detected TZ cancer were identified in the total population of 130 patients. To ensure that more than 90% of at least one MR spectroscopic imaging voxel included tumor, we restricted the patient population to those 20 patients in whom the pathology step-section map showed a TZ tumor of 1 cm or greater in largest in-plane diameter. Data from four of these patients were eliminated from MR spectroscopic imaging analysis because most or all of the tumor was far anterior and was not included in the PRESS excitation volume; this yielded 16 patients with TZ tumors for quantitative analysis. Age, presurgical prostate-specific antigen (PSA) level, and clinical stage were recorded for each patient.

Quantitative Analysis of MR Spectroscopic Imaging Data

A radiologist (H.H.) with over 10 years of experience interpreting endorectal MR images of the prostate matched the whole-mount pathology step sections with the most closely corresponding MR images and identified the tumor region of interest in the images. Only MR spectroscopic imaging voxels with more than 90% of their volume contained within the tumor region of interest were considered "tumor" voxels. The metabolites studied were those resonating at approximately 3.22 parts per million (ppm) (ie, Cho, a peak that can have contributions from free choline, phosphocholine, glycerophosphocholine, ethanolamine, phosphoethanolamine, spermine, and taurine and that is dominated by the tri-methyl protons of choline and phosphocholine [15,24]), 3.02 ppm (ie, Cr), and 2.62 ppm (ie, Cit).

The normalized peak areas for Cho, Cr, and Cit for each tumor voxel were tabulated and used to calculate the following ratios: (Cho + Cr)/Cit, Cho/Cr, and Cho/Cit. For a voxel to be considered diagnostic in this study, at least one of the metabolites (Cho, Cr, or Cit) was required to have a signal-to-noise ratio of 2:1 or higher. In addition, any metabolite with a signal-to-noise ratio less than 1 was simply assigned the noise value. For each patient, the mean value of each ratio in the tumor region of interest was calculated. "Benign control" voxels were chosen randomly from the set of TZ MR spectroscopic imaging voxels that did not contain tumor and were not adjacent to tumor or the urethra. Whenever possible, the number of control voxels was made equal to the number of tumor voxels. For some patients with very large TZ tumors, there were fewer control voxels than tumor voxels. The number of voxels in tumor regions ranged from one to 47 in the 16 patients, while the number of control voxels ranged from one to 25. In addition to metabolite ratios, the number of voxels in which only Cho was detectable (with a signal-to-noise ratio of 2:1 or higher) was assessed. Finally, in both tumor and control regions, the percentage of voxels that contained no detectable metabolites was tabulated.

Statistical Analysis

Wilcoxon signed rank tests were used to compare tumor with control tissue for each of the following variables: (Cho + Cr)/Cit, Cho/Cr, and Cho/Cit. In each

Clinical and Pathologic Data for 16 Patients with TZ Tumors

Patient No./Age (y)	PSA Level (ng/mL)	Clinical Stage	Pathologic Stage	Gleason Score for Gland	Gleason Score for TZ Tumor	Tumor Origin
1/62	8.7	T1c	T2bN0M0	3 + 4	3 + 3	TZ
2/50	2.9	T2a	T2bN0M0	3 + 3	3 + 3	PZ*
3/51	6.1	T2b	T2bN0M0	3 + 4	3 + 4	TZ
4/68	28.4	T1c	T2bN0M0	3 + 3 + focal 4†	3 + 3	PZ*
5/51	4.5	T1c	T2bN0M0	3 + 4	3 + 4	PZ*
6/53	3.8	T1c	T4N0M0	3 + 3	3 + 3	TZ
7/55‡	4.93	T3a	T3aN0M0	3 + 4	3 + 3	TZ
8/56	12.0	T2c	T2bN0M0	3 + 4	3 + 4	TZ
9/54	4.8	T2a	T2bN0M0	3 + 4	3 + 4	TZ
10/51	6.9	T2b	T3bN0M0	4 + 3	3 + 3	TZ
11/63	8.7	T2a	T2bN0M0	3 + 4	3 + 4	TZ
12/58	5.5	T1c	T4N0M0	3 + 4	3 + 4	TZ
13/62	4.7	T2a	T2bN0M0	3 + 4	3 + 3	PZ*
14/59	9.8	T2a	T2bN0M0	3 + 3	3 + 3	TZ
15/63	9.3	T2a	T4N0M0	3 + 4	3 + 3	TZ
16/61	11.0	T2c	T2bN0M0	4 + 3	4 + 3	Indeterminate§

* Origin in PZ but large component in TZ.
† Gleason 4 component less than 5%.
‡ Only patient without at least one synchronous tumor in PZ.
§ Unclear whether origin was TZ or PZ.

case, cancer tissue was paired with normal tissue for each patient. The significance of detecting just Cho in tumor voxels versus control voxels and the significance of detecting no metabolites were assessed with the McNemar test (25). A *P* value of less than .05 was considered to indicate a statistically significant difference.

RESULTS

The Table contains a summary of the clinical and pathologic information from the 16 patients evaluated in the quantitative study. The mean age of the population was 57.3 years ± 5.5 (SD). The mean pretreatment PSA level was 8.25 ± 6.02, and the mean Gleason score for the gland (as evaluated after radical prostatectomy) was 6.62 ± 0.50. Nine patients had only a Gleason 3 component in their TZ tumors, while seven had both Gleason 3 and Gleason 4 components. There were 11 tumors of TZ origin, four of PZ origin with large TZ components, and one with a large TZ component whose origin could not be determined. Of the 16 patients, 15 had at least one focus of PZ cancer in addition to the TZ tumor.

The mean (Cho + Cr)/Cit, Cho/Cr, and Cho/Cit ratios in tumor and control regions for the 16 patients are illustrated in Figure 1. The following differences were found: The mean (Cho + Cr)/Cit ratio was 1.74 ± 1.35 (SD) in tumor tissue versus 0.63 ± 0.20 in control tissue (P = .001), the mean Cho/Cr ratio was 3.01 ± 1.61 in tumor tissue versus 1.70 ± 0.89 in control tissue (P = .003), and the mean Cho/Cit ratio was 1.28 ± 1.16 in tumor tissue versus 0.35 ± 0.11 in control tissue (P = .001). These findings indicate that TZ tumors tend to have higher Cho and lower Cr and Cit levels than benign TZ tissue. This is illustrated in Figure 2, which shows data from a patient with a large TZ tumor in the left side of the prostate. The spectra indicate that the patient's PZ in this plane was healthy appearing, with high levels of Cit and low levels of Cho plus Cr. Voxels within the TZ tumor region showed comparatively high levels of Cho and little or no detectable Cr or Cit. The tumor was composed mostly of Gleason 3 tissue, with a small percentage of Gleason 4 tissue.

The data in Figure 1 indicate that there was substantial overlap between some tumor metabolite ratios and control ratios. In Figure 3, the variability of the proton metabolic profile in BPH, which was a possible factor in this overlap, is evident. In the glandular BPH region, the amount of Cit is high, while in the stromal region, the Cit level is much lower, demonstrating the variability of Cit content in the TZ. The patient described in Figure 3 also had a large anterior TZ tumor, which, in the plane in which Figure 3a was acquired, was almost entirely excluded from the PRESS excitation volume. At the time of our study, the excitation volume was selected to include the entire PZ while excluding as much periprostatic lipid as possible; this resulted in the exclusion of some of the TZ tumor. Figure 4 shows a more inferior transverse MR imaging section obtained in the same patient for which, owing to the orientation of the gland, the excitation volume included more of the anterior TZ tumor. The metabolic profile revealed that this tumor had elevated Cho and low or absent Cr and Cit levels—similar to the tumor shown in Figure 2.

Nine (56%) of the 16 patients had at least one tumor voxel in which Cho was the only detectable peak. For the tumor whose spectra are shown in Figure 2b, Cho was the only detectable peak in several voxels. No control (ie, BPH) voxels in which only Cho was detectable were found for any patient. Results of McNemar testing indicated that Cho-only expression in tumor tissue was significantly higher than that seen in control tissue (P = .008). The percentage of voxels with no detectable metabolites did not significantly differ for cancer tissue versus control tissue (P = .134).

DISCUSSION

To our knowledge, this is the first in vivo ^{1}H MR spectroscopic imaging study focused specifically on TZ tumors. Differentiation of tumor from BPH with imaging modalities such as US and MR imaging has been problematic (12,13,26,27). BPH has been described as "multiple tissue nodules that express a wide spectrum of gland density and activity . . . separated by widely variable quantities of internodular tissue showing a range of atrophic changes" (28). On the basis of this description, hypertrophied TZ tissue might also be expected to demonstrate

metabolic heterogeneity, which could complicate its differentiation from cancer.

In vitro MR studies of prostate tissue extracts have been performed on transurethral and radical prostatectomy specimens (16,29–33). Proton MR has revealed, on average, elevated Cit levels in BPH tissue as compared with human prostate cancer in unspecified zones (29,30,32) and human prostate cancer in the PZ (33). However, the Cit level in BPH has been found to positively correlate with the percentage of glandular tissue in the specimen, and some stromal BPH tissue has been observed to contain levels of Cit comparable to those in cancer tissue (33). Kurhanewicz et al (16,30) and Cornel et al (32) reported higher levels of Cho in cancer than in BPH, while Schiebler et al (33) found no difference between choline content in cancer and in BPH. Cancer has also been shown to have lower levels of phosphoethanolamine than BPH (16,30,32). In a study involving phosphorus 31 (^{31}P) MR spectroscopy, a lower ratio of phosphoethanolamine to phosphocholine was observed in human prostate cancer grown in nude mice and in a high-grade human tumor as compared with that in BPH (31,32). On the basis of results of extract studies, Cit content and the ratios of Cit to total choline, Cit to lactate, phosphocholine to total creatine, choline to total creatine, and phosphoethanolamine to phosphocholine have been suggested as in vivo markers for differentiating BPH from prostate cancer (30–32).

Improved hardware has permitted in vivo MR studies that have provided information on prostate cancer, BPH, and normal tissue (15,31,34–36). Results of an early ^{31}P MR study showed that prostate glands from patients with BPH had elevated phosphomonester/nucleotide triphosphate levels compared with normal prostates (31). Localized proton MR techniques such as PRESS (22) and STEAM (stimulated-echo acquisition mode) (37), more recently combined with chemical shift imaging (23), have been used for further characterizing zonal anatomy in normal tissue and in disease (15,16,35,36). Healthy young volunteers with no BPH have been found to have a significantly lower Cit content in the central zone of the prostate than in the PZ (35,36). Results of ^{1}H MR spectroscopic imaging have shown that glandular BPH nodules have Cit levels comparable to those in normal, healthy PZ tissue, while stromal BPH regions have reduced Cit levels that are in some cases similar to those in PZ cancers identified at MR imaging (15). Choline in BPH has been found to be elevated compared with choline in normal PZ tissue (15,16). Compared with levels in cancers of the PZ, mean Cho, Cr, and (Cho + Cr)/Cit levels in BPH have been found to differ significantly; however, overlap was substantial (15).

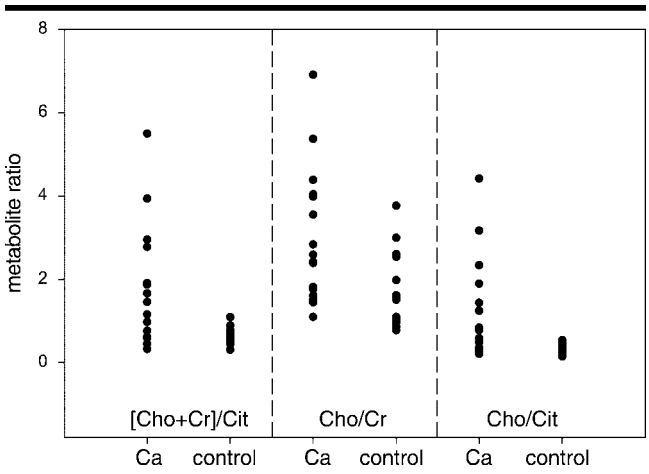

Figure 1. Scatterplot depicts average metabolite ratios for 16 patients in cancerous TZ regions *(Ca)* and benign control regions.

The present study was focused on TZ tumors that were identified at step-section histopathologic examination and were spatially correlated with T2-weighted MR images and MR spectroscopic images. Although previous prostate cancer extract studies were not specifically focused on TZ tumors, the trend of reduced Cit and elevated Cho levels seen in those studies agrees with the results of this in vivo study (29,30,32,33). In addition, the difference in (Cho + Cr)/Cit values between TZ cancer and BPH observed in the present study is similar to that observed between PZ cancers and BPH in a previous in vivo study (15). We suspect that the difference between TZ tumor and BPH metabolite ratios arises from both a reduction of Cit and an elevation of Cho in the tumor. It has been suggested that tumor cells, as compared with normal prostatic epithelium, have increased oxidation of Cit (38). Cho are constituents of membrane synthesis and degradation pathways and have been found to be elevated in many cancers (39–45). One possible reason for this elevation is increased cell proliferation (46–48).

Although one might have expected a wide range of (Cho + Cr)/Cit and Cho/Cit values in BPH voxels owing to variations in Cit levels, tumor ratios in the present study showed even greater variability. It has been shown in vitro that prostate tumor tissue samples containing no normal epithelial cells had no detectable Cit, while tumor samples containing nonmalignant epithelial cells contained substantial amounts of Cit (32). In our study, because the presence of normal or nonmalignant cells within a tumor voxel could not be ruled out, Cit may have been present to some degree. Also, although data were restricted to larger tumors that filled more than 90% of the voxel, some volume averaging of tumor with benign glandular tissue may have occurred. The level of Cho may vary with tumor grade (49). However, the small number of patients in the present study did not permit stratification on the basis of tumor grade.

The relatively close grouping of (Cho + Cr)/Cit and Cho/Cit in benign voxels that was observed in this study could have been caused in part by the elimination of voxels with no detectable metabolites—presumably those in stromal regions. This would have biased the benign voxel (Cho + Cr)/Cit and Cho/Cit ratios toward lower values (higher Cit). The Cho/Cr ratios in tumor and control voxels showed large variations and overlapped considerably, possibly due to the low signal-to-noise ratio of the Cr peak. In addition, Cho and Cr are not always well resolved, adding to the uncertainty.

In the PZ, (Cho + Cr)/Cit values in benign tissue and cancer tissue have been shown to not only be statistically different but also to have very little overlap (15,50). However, in the cases of TZ cancer evaluated in our study, there was substantial overlap between metabolite ratios in tumor and those in benign tissue, and choosing a cutoff value of (Cho + Cr)/Cit or Cho/Cit for differentiating cancer would result in some cancers go-

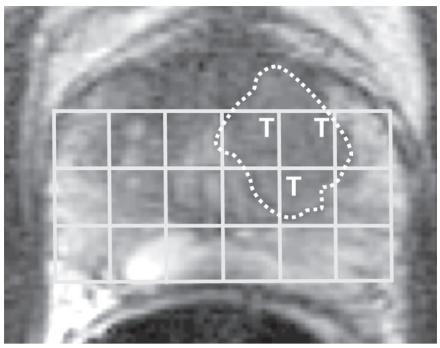

a.

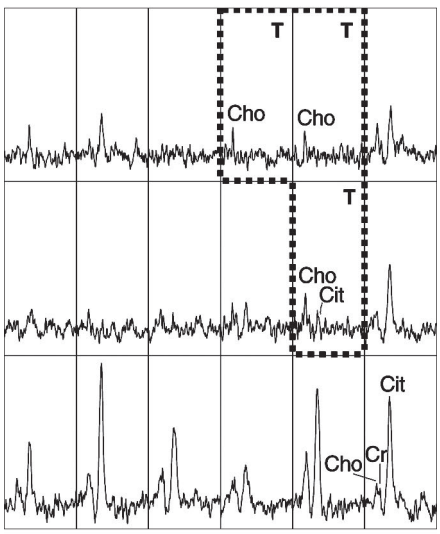

b.

c.

Figure 2. MR imaging/MR spectroscopic imaging data and pathology section in a 51-year-old patient (patient 5) with a large left-sided TZ tumor. The patient also had a small tumor in the right side of the PZ. **(a)** MR spectroscopic imaging grid superimposed on transverse T2-weighted MR image obtained with 1,000/130, PRESS volume excitation with BASING water and lipid suppression, 16 × 8 × 8 chemical shift imaging, a 100 × 50 × 50-mm field of view, 6.25-mm resolution, one signal acquired, and a 17-minute imaging time shows tumor *(T)* in dashed region. **(b)** Spectral grid corresponding to **a** shows metabolite levels. *T* and dashed lines indicate tumor regions. **(c)** Whole-mount pathology step section shows tumor regions (outlined).

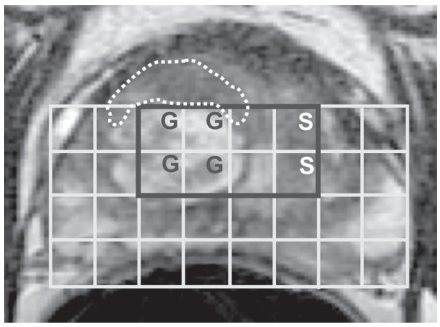

a.

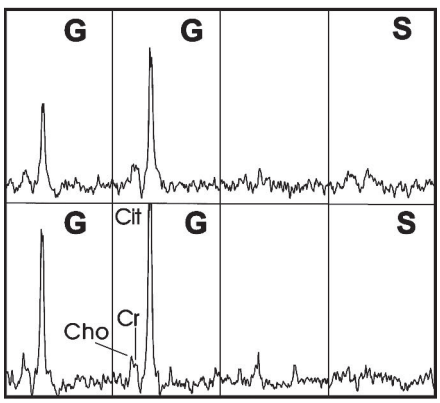

b.

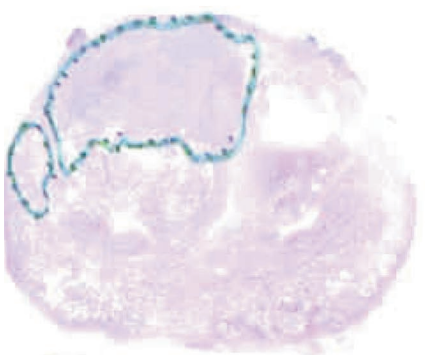

c.

Figure 3. MR imaging/MR spectroscopic imaging data and pathology section in a 56-year-old patient (patient 8) with glandular BPH, stromal BPH, and TZ tumor. **(a)** MR spectroscopic imaging grid superimposed on transverse T2-weighted MR image obtained with 1,000/130, PRESS volume excitation with BASING water and lipid suppression, 16 × 8 × 8 chemical shift imaging, a 100 × 50 × 50-mm field of view, 6.25-mm resolution, one signal acquired, and a 17-minute imaging time shows tumor, which is indicated by dashed line. *G* = glandular BPH, *S* = stromal BPH. **(b)** Subgrid of spectra corresponding to the black rectangular region in **a**. *G* = glandular BPH, *S* = stromal BPH. **(c)** Pathology step section corresponding most closely to **a** shows tumor regions (outlined).

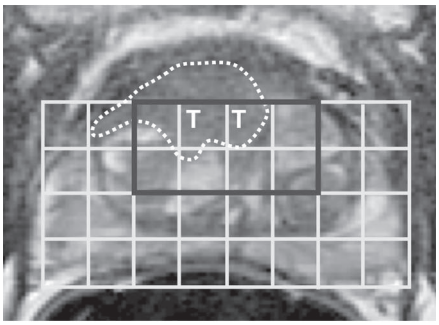

a.

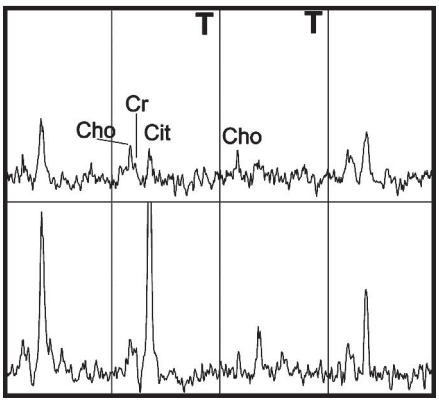

b.

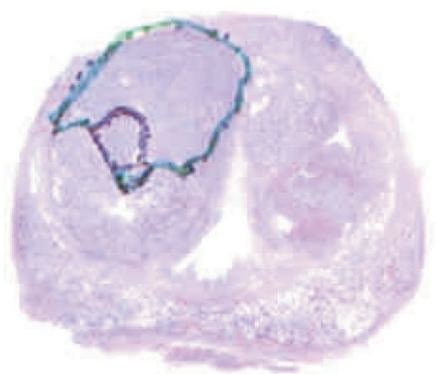

c.

Figure 4. MR imaging/MR spectroscopic imaging data obtained in the same patient as in Figure 3 but at a more inferior location. **(a)** MR spectroscopic imaging grid superimposed on transverse T2-weighted MR image obtained with 1,000/130, PRESS volume excitation with BASING water and lipid suppression, 16 × 8 × 8 chemical shift imaging, a 100 × 50 × 50-mm field of view, 6.25-mm resolution, one signal acquired, and a 17-minute imaging time shows tumor *(T)* surrounded by dashed line. **(b)** Subgrid of spectra corresponding to the black rectangular region in **a**. *T* = tumor. **(c)** Pathology step section corresponding most closely to **a** shows tumor regions (outlined).

ing undetected. On the basis of the data in this study, the metabolic characteristic most likely to indicate TZ cancer is the presence of at least one voxel in which Cho is the only detectable metabolite peak.

While demonstrating the proton metabolic characteristics of TZ tumors, the results of this study also illuminated the technical difficulties involved in evaluating the TZ with MR spectroscopic imaging. For high-resolution MR spectroscopic imaging (6.25-mm in-plane resolution), an endorectal probe is used to achieve adequate signal-to-noise ratio within a clinically feasible imaging time. However, the anterior portion of the prostate gland, which is most distant from the probe, can still have relatively low signal-to-noise ratio on such images. Indeed, the signal-to-noise threshold level used in the present study was lower than that used previously in studies of the PZ (8,51). However, because this is the current technological limit, the lower threshold and the possibility of increased scatter in the data were accepted. Coverage of the anterior gland at MR spectroscopic imaging was purposefully restricted because *(a)* the PZ was the main region of clinical interest and *(b)* excitation of anterior periprostatic lipids can result in lipid contamination artifacts in MR spectroscopic imaging data. Therefore, tumors that were very anterior were in some cases partially or completely excluded from the excitation volume. Finally, the TZ is immediately adjacent to the urethra, which can contain glycerophosphocholine in seminal fluid (52). Glycerophosphocholine resonates in the choline region, making detection of TZ cancer adjacent to the urethra difficult.

Despite the difficulties in assessing the TZ, the benefits could be substantial. Currently, the PZ is targeted at most biopsies. It is not uncommon for a patient to be strongly suspected of having prostate cancer on the basis of a rising PSA level and yet have negative biopsy results (sometimes after multiple biopsy attempts) because the cancer is in the TZ. In fact, it has been suggested that patients with multiple negative biopsy results and an elevated and/or rising PSA level should undergo biopsies in which the TZ is specifically targeted (53). Even when the TZ is specifically targeted at biopsy, smaller tumors (<2 cm^3) may be missed (28). Accurate imaging guidance could help improve positive yield for TZ biopsies. TZ tumors are more likely to be organ confined, have a lower Gleason score, and have higher biochemical cure rates than same-volume PZ tumors (13,54). Even quite large TZ tumors (7–86 cm^3) are more likely to remain organ confined (55). Thus, if patients with single or dominant TZ tumors can be given a confident diagnosis with use of an imaging modality, they may be candidates for alternative therapies or watchful waiting, depending on other clinical considerations.

In the present study, we assessed only the MR spectroscopic imaging parameters of TZ cancers. Features indicating the presence of TZ tumors on T2-weighted MR images have recently been reported (56,57). In addition, dynamic contrast material–enhanced MR imaging may show promise for differentiating cancer from BPH (57,58). Recent technical improvements, including outer volume saturation pulses (59) and the ability to prescribe oblique MR spectroscopic imaging volumes, should permit the assessment of the entire TZ. With currently available technology, it is important that the TZ not be overlooked during prostate staging evaluation with MR imaging/MR spectroscopic imaging.

In summary, although a trend toward elevation of Cho and reduction in or lack of Cit was observed in TZ tumors when they were compared with BPH, the broad range of metabolite ratios observed precludes the use of a single ratio to differentiate TZ cancer from benign TZ tissue. A prospective study is now needed to ascertain the value of combined MR imaging/MR spectroscopic imaging in the detection of TZ tumors.

Acknowledgment: The authors thank the investigators of the Magnetic Resonance Science Center at the University of California at San Francisco for the use of their data acquisition and processing software.

References

1. Adusumilli S, Pretorius ES. Magnetic resonance imaging of prostate cancer. Semin Urol Oncol 2002; 20:192–210.
2. Engelbrecht MR, Jager GJ, Laheij RJ, Verbeek AL, Van Lier HJ, Barentsz JO. Local staging of prostate cancer using magnetic resonance imaging: a meta-analysis. Eur Radiol 2002; 12:2294–2302.
3. Cornud F, Flam T, Chauveinc L, et al. Extraprostatic spread of clinically localized prostate cancer: factors predictive of pT3 tumor and of positive endorectal MR imaging examination results. Radiology 2002; 224:203–210.
4. Clarke DH, Banks SJ, Wiederhorn AR, et al. The role of endorectal coil MRI in patient selection and treatment planning for prostate seed implants. Int J Radiat Oncol Biol Phys 2002; 52:903–910.
5. Soulie M, Aziza R, Escourrou G, et al. Assessment of the risk of positive surgical margins with pelvic phased-array magnetic resonance imaging in patients with clinically localized prostate cancer: a prospective study. Urology 2001; 58:228–232.
6. D'Amico AV, Schnall M, Whittington R, et al. Endorectal coil magnetic resonance imaging identifies locally advanced prostate cancer in select patients with clinically localized disease. Urology 1998; 51: 449–454.
7. Schiebler ML, Schnall MD, Pollack HM, et al. Current role of MR imaging in the staging of adenocarcinoma of the prostate. Radiology 1993; 189:339–352.
8. Kurhanewicz J, Vigneron DB, Hricak H, et al. Prostate cancer: metabolic response to cryosurgery as detected with 3D H-1 MR spectroscopic imaging. Radiology 1996; 200:489–496.
9. Kurhanewicz J, Males R, Sokolov D, et al. Combined endorectal/phased-array MR imaging and 3-D 1H-MR spectroscopic imaging for improved diagnosis of extracapsular extension in prostate cancer (abstr). In: Proceedings of the Sixth Meeting of the International Society for Magnetic Resonance in Medicine. Berkeley, Calif: International Society for Magnetic Resonance in Medicine, 1998; 967.
10. Scheidler J, Hricak H, Vigneron DB, et al. Prostate cancer: localization with three-dimensional proton MR spectroscopic imaging—clinicopathologic study. Radiology 1999; 213:473–480.
11. McNeal JE, Redwine EA, Freiha FS, Stamey TA. Zonal distribution of prostatic adenocarcinoma: correlation with histologic pattern and direction of spread. Am J Surg Pathol 1988; 12:897–906.
12. Ikonen S, Kivisaari L, Tervahartiala P, Vehmas T, Taari K, Rannikko S. Prostatic MR imaging: accuracy in differentiating cancer from other prostatic disorders. Acta Radiol 2001; 42:348–354.
13. Noguchi M, Stamey TA, Neal JE, Yemoto CE. An analysis of 148 consecutive transition zone cancers: clinical and histological characteristics. J Urol 2000; 163:1751–1755.
14. Kaji Y, Kurhanewicz J, Hricak H, et al. Localizing prostate cancer in the presence of postbiopsy changes on MR images: role of proton MR spectroscopic imaging. Radiology 1998; 206:785–790.
15. Kurhanewicz J, Vigneron DB, Hricak H, Narayan P, Carroll P, Nelson SJ. Three-dimensional H-1 MR spectroscopic imaging of the in situ human prostate with high (0.24–0.7-cm^3) spatial resolution. Radiology 1996; 198:795–805.
16. Kurhanewicz J, Vigneron DB, Nelson SJ, Hricak H. Citrate as an in vivo marker to discriminate prostate cancer from benign prostatic hyperplasia and normal prostate peripheral zone: detection via localized proton spectroscopy. Urology 1995; 45:459–466.
17. Males R, Vigneron D, Nelson S, et al. Addition of MR spectroscopic imaging to MRI significantly improves detection and localization of prostate cancer (abstr). In: Proceedings of the Sixth Meeting of the International Society for Magnetic Resonance in Medicine. Berkeley, Calif: International Society for Magnetic Resonance in Medicine, 1998; 487.
18. Star-Lack J, Nelson SJ, Kurhanewicz J, Huang LR, Vigneron DB. Improved water and lipid suppression for 3D PRESS CSI using RF band selective inversion with gradient dephasing (BASING). Magn Reson Med 1997; 38:311–321.
19. Moyher SE, Vigneron DB, Nelson SJ. Surface coil MR imaging of the human brain with an analytic reception profile correc-

tion. J Magn Reson Imaging 1995; 5:139–144.
20. Vigneron DB, Nelson SJ, Moyher S, Kelley D, Kurhanewicz J, Hricak H. An analytical correction of MR images obtained with endorectal or surface coils. J Magn Reson Imaging 1993; 3:142–145.
21. Nelson SJ, Day MR, Carvajal L. Methods for analysis of serial volume MRI and ^{1}H MRS data for the assessment of response to therapy in patients with brain tumors (abstr). In: Proceedings of the Society of Magnetic Resonance in Medicine and the European Society of Magnetic Resonance in Medicine and Biology. Berkeley, Calif: Society of Magnetic Resonance in Medicine, 1995; 1960.
22. Bottomley P. Selective volume method for performing localized NMR spectroscopy. U.S. patent no. 4,480,228. 1984.
23. Brown TR, Kincaid BM, Ugurbil K. NMR chemical shift imaging in three dimensions. Proc Natl Acad Sci U S A 1982; 79:3523–3526.
24. van der Graaf M, Schipper RG, Oosterhof GO, Schalken JA, Verhofstad AA, Heerschap A. Proton MR spectroscopy of prostatic tissue focused on the detection of spermine, a possible biomarker of malignant behavior in prostate cancer. MAGMA 2000; 10:153–159.
25. Conover WJ. Practical nonparametric statistics. 2nd ed. New York, NY: Wiley, 1980.
26. Griebel J, Hess CF, Schmiedl U, Koelbel G. MR characteristics of prostatic carcinoma and benign prostatic hyperplasia at 1.5 T. J Comput Assist Tomogr 1988; 12:988–994.
27. Schiebler ML, Tomaszewski JE, Bezzi M, et al. Prostatic carcinoma and benign prostatic hyperplasia: correlation of high-resolution MR and histopathologic findings. Radiology 1989; 172:131–137.
28. McNeal J, Noldus J. Limitations of transition zone needle biopsy findings in the prediction of transition zone cancer and tissue composition of benign nodular hyperplasia. Urology 1996; 48:751–756.
29. Fowler AH, Pappas AA, Holder JC, et al. Differentiation of human prostate cancer from benign hypertrophy by in vitro 1H NMR. Magn Reson Med 1992; 25:140–147.
30. Kurhanewicz J, Dahiya R, Macdonald JM, Chang LH, James TL, Narayan P. Citrate alterations in primary and metastatic human prostatic adenocarcinomas: ^{1}H magnetic resonance spectroscopy and biochemical study. Magn Reson Med 1993; 29:149–157.
31. Narayan P, Jajodia P, Kurhanewicz J, et al. Characterization of prostate cancer, benign prostatic hyperplasia and normal prostates using transrectal 31-phosphorus magnetic resonance spectroscopy: a preliminary report. J Urol 1991; 146:66–74.
32. Cornel EB, Smits GAHJ, Oosterhof GON, et al. Characterization of human prostate cancer, benign prostatic hyperplasia, and normal prostate by in vitro ^{1}H and ^{31}P magnetic resonance spectroscopy. J Urol 1993; 150:2019–2024.
33. Schiebler ML, Miyamoto KK, White M, Maygarden SJ, Mohler JL. In vitro high resolution 1H-spectroscopy of the human prostate: benign prostatic hyperplasia, normal peripheral zone and adenocarcinoma. Magn Reson Med 1993; 29:285–291.
34. Schick F, Bongers H, Kurz S, Jung WI, Pfeffer M, Lutz O. Localized proton MR spectroscopy of citrate in vitro and of the human prostate in vivo at 1.5 T. Magn Reson Med 1993; 29:38–43.
35. Lowry M, Liney GP, Turnbull LW, Manton DJ, Blackband SJ, Horsman A. Quantification of citrate concentration in the prostate by proton magnetic resonance spectroscopy: zonal and age-related differences. Magn Reson Med 1996; 36:352–358.
36. Heerschap A, Jager GJ, van der Graaf M, Barentsz JO, Ruijs SH. Proton MR spectroscopy of the normal human prostate with an endorectal coil and a double spin-echo pulse sequence. Magn Reson Med 1997; 37:204–213.
37. Frahm J, Bruhn H, Gyngell MNL, Merboldt KD, Hanicke W, Sauter R. Localized high-resolution proton NMR spectroscopy using stimulated echoes: initial applications to human brain in vivo. Magn Reson Med 1989; 9:79–93.
38. Costello LC, Littleton GK, Franklin RB. Regulation of citrate-related metabolism in normal and neoplastic prostate. In: Sharma RK, Criss WE, eds. Endocrine control in neoplasia. New York, NY: Raven, 1978; 303–314.
39. Fulham MJ, Bizzi A, Dietz MJ, et al. Mapping of brain tumor metabolites with proton MR spectroscopic imaging: clinical relevance. Radiology 1992; 185:675–686.
40. McBride DQ, Miller BL, Nikas DL, et al. Analysis of brain tumors using ^{1}H magnetic resonance spectroscopy. Surg Neurol 1995; 44:137–144.
41. Heesters MA, Kamman RL, Mooyaart EL, Go KG. Localized proton spectroscopy of inoperable brain gliomas: response to radiation therapy. J Neurooncol 1993; 17: 27–35.
42. Sijens PE, Knopp MV, Brunetti A, et al. ^{1}H MR spectroscopy in patients with metastatic brain tumors: a multicenter study. Magn Reson Med 1995; 33:818–826.
43. Rutter A, Hugenholtz H, Saunders JK, Smith ICP. One-dimensional phosphorus-31 chemical shift imaging of human brain tumors. Invest Radiol 1995; 30:359–366.
44. Koutcher JA, Ballon D, Graham M, et al. P-31 NMR spectra of extremity sarcoma: diversity of metabolic profiles and changes in response to chemotherapy. Magn Reson Med 1990; 16:19–34.
45. Dewhirst MW, Sostman HD, Leopold KA, et al. Soft-tissue sarcomas: MR imaging and MR spectroscopy for prognosis and therapy monitoring—work in progress. Radiology 1990; 174:847–853.
46. Daly PF, Lyon RC, Faustino PJ, Cohen JS. Phospholipid metabolism in cancer cells monitored by 31P NMR spectroscopy. J Biol Chem 1987; 262:14875–14878.
47. Shimizu H, Kumabe T, Shirane R, Yoshimoto T. Correlation between choline level measured by proton MR spectroscopy and Ki-67 labeling index in gliomas. AJNR Am J Neuroradiol 2000; 21:659–665.
48. Smith TA, Eccles S, Ormerod MG, Tombs AJ, Titley JC, Leach MO. The phosphocholine and glycerophosphocholine content of an oestrogen-sensitive rat mammary tumour correlates strongly with growth rate. Br J Cancer 1991; 64:821–826.
49. Kurhanewicz J, Vigneron DB, Nelson SJ. Three-dimensional magnetic resonance spectroscopic imaging of brain and prostate cancer. Neoplasia 2000; 2:166–189.
50. Males R, Vigneron D, Star-Lack J, et al. Clinical application of BASING and spectral/spatial water and lipid suppression pulses for prostate cancer staging and localization by in vivo 3D 1H magnetic resonance spectroscopic imaging. Magn Reson Med 2000; 43:17–22.
51. Yu KK, Scheidler J, Hricak H, et al. Prostate cancer: prediction of extracapsular extension with endorectal MR imaging and three-dimensional proton MR spectroscopic imaging. Radiology 1999; 213:481–488.
52. Kurhanewicz J, Dahiya R, Macdonald JM, et al. Phosphorus metabolite characterization of human prostatic adenocarcinoma in a nude mouse model by 31P magnetic resonance spectroscopy and high pressure liquid chromatography. NMR Biomed 1992; 5:185–192.
53. Liu IJ, Macy M, Lai YH, Terris MK. Critical evaluation of the current indications for transition zone biopsies. Urology 2001; 57:1117–1120.
54. Greene DR, Wheeler TM, Egawa S, Dunn JK, Scardino PT. A comparison of the morphological features of cancer arising in the transition zone and in the peripheral zone of the prostate. J Urol 1991; 146:1069–1076.
55. Stamey TA, Dietrick DD, Issa MM. Large, organ confined, impalpable transition zone prostate cancer: association with metastatic levels of prostate specific antigen. J Urol 1993; 149:510–515.
56. Eberhardt SC, Coakley FV, Schwartz LH, Zakian KL, Heinze SB, Hricak H. Endorectal MR imaging and spectroscopic imaging of transition zone prostate cancer (abstr). Radiology 2001; 221(P):584.
57. Kitamura Y, Kaji Y, Li H, Manabe T, Sugimura K, Tachibana M. Prostate cancer derived from transition zone specific findings on MR imaging. Presented at the Ninth Annual Symposium on Urogenital Radiology of the European Society of Urogenital Radiology, Genoa, Italy, June 15–20, 2002.
58. Turnbull LW, Buckley DL, Turnbull LS, Liney GP, Knowles AJ. Differentiation of prostatic carcinoma and benign prostatic hyperplasia: correlation between dynamic Gd-DTPA-enhanced MR imaging and histopathology. J Magn Reson Imaging 1999; 9:311–316.
59. Tran T, Vigneron D, Sailasuta N, et al. Very selective suppression pulses for clinical MRSI studies of brain and prostate cancer. Magn Reson Med 2000; 43:23–33.